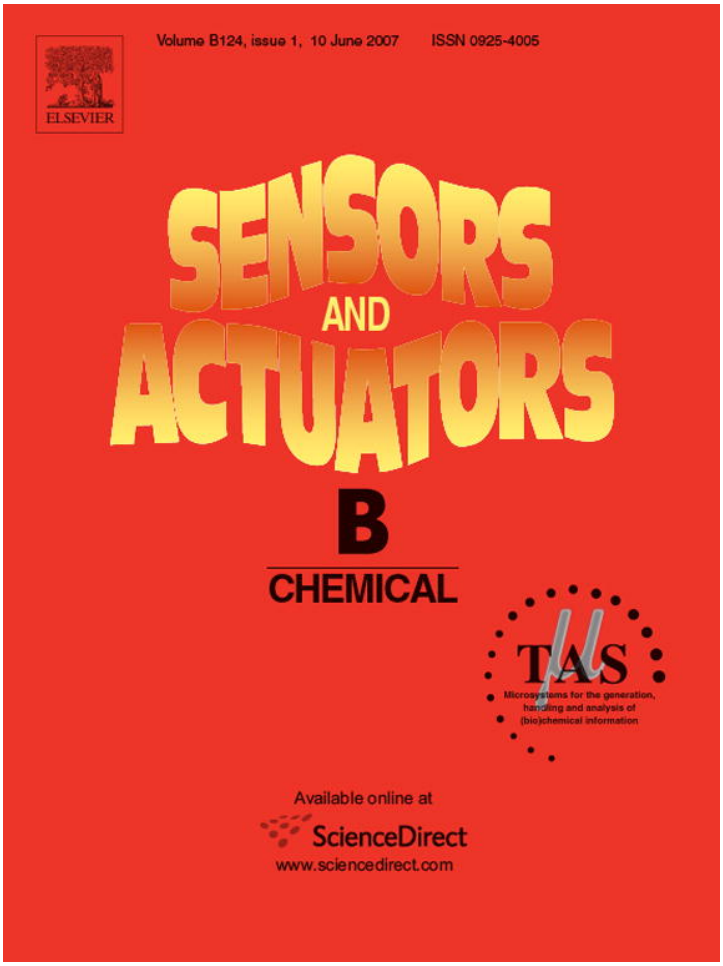

Available online at www.sciencedirect.com
ScienceDirect
Sensors and Actuators B 124 (2007) 133–142
SENSORS AND ACTUATORS B CHEMICAL
www.elsevier.com/locate/snb

# Structural distinctions of $Fe_2O_3$–$In_2O_3$ composites obtained by various sol–gel procedures, and their gas-sensing features

Maria I. Ivanovskaya [a,*], Dzmitry A. Kotsikau [a], Antonietta Taurino [b], Pietro Siciliano [b]

[a] *Research Institute for Physical Chemical Problems, Belarusian State University, 14 Leningradskaya, 220030 Minsk, Belarus*
[b] *Institute of Microelectronics and Microsystems, IMM-CNR, Lecce Department, Via Arnesano, 73100 Lecce, Italy*

Received 21 July 2006; received in revised form 5 December 2006; accepted 6 December 2006
Available online 8 January 2007

**Abstract**

New and various approaches to the sol–gel synthesis of advanced gas-sensing materials based on nanosized $Fe_2O_3$–$In_2O_3$ (9:1 mol) mixed oxides, which differ in phase composition and grain size, have been considered in this paper. The correlation between the structural features of the composites and their gas-sensing behavior has been established. It was found that multi-phase $Fe_2O_3$–$In_2O_3$ composites containing metastable γ-$Fe_2O_3$ structure are characterized by the greatest sensitivity to both reducing ($C_2H_5OH$) and oxidizing ($NO_2$) gases tested in this paper. The influence of synthesis conditions on the structural peculiarities of the $Fe_2O_3$–$In_2O_3$ composites was studied in detail and the possibility to adjust fine structure of the materials was demonstrated.


*Keywords:* $Fe_2O_3$–$In_2O_3$ nano-composites; $C_2H_5OH$ and $NO_2$ gas sensors; Structural characterization

## 1. Introduction

Composites based on iron and indium oxides are widely used as active layers of semiconducting gas sensors. The gas-sensing behavior of $Fe_2O_3$–$In_2O_3$-based sensors is essentially determined by the phase composition of the oxides, their dispersity and the $Fe_2O_3$ concentration [1–5].

A substantial literature on this topic has been published; $Fe_2O_3$–$In_2O_3$ films containing γ-$Fe_2O_3$ modification of iron oxide are reported to be more sensitive to $O_3$ than α-$Fe_2O_3$-based films [6]. $Fe_2O_3$–$In_2O_3$ films with α-$Fe_2O_3$ as a main phase exhibit an enhanced response to $C_2H_5OH$ vapors as compared to $In_2O_3$ films slightly doped with $Fe_2O_3$ [1]. Chibirova and Gutman showed that the functional (in particular, gas-sensing) features of $Fe_2O_3$-based oxides strongly depend on their pre-history, i.e. on the preparation procedure and mode of thermal treatment [7].

Nevertheless, a detailed structural distinction between the $Fe_2O_3$–$In_2O_3$ films in relation to their dissimilar gas-sensing behavior has not been considered before.

In this paper, the structural peculiarities of $Fe_2O_3$–$In_2O_3$ nanosized composites have been studied depending on the synthesis conditions and annealing temperature in order to assess the deposition parameters, which allow to obtain different structural modifications of $Fe_2O_3$ with different gas-sensing features.

The samples were obtained by inorganic modification of the sol–gel technology, which is based on the use of inorganic metal salts as precursors, as opposed to the classical modification using organic metal derivatives. The inorganic approach gives the possibility to prepare oxide composites in a nanosized state and to attain considerable mutual solubility of the components. It is worth noting that the used technology allows also to widely vary the phase composition and fine structure of the samples and therefore to control their gas-sensing characteristics.

## 2. Experimental

$Fe_2O_3$–$In_2O_3$ samples with a Fe:In = 9:1 molar ratio and various phase composition were studied along with individual iron and indium oxides. The 9:1 molar ratio was found to be the most promising for gas-sensing applications [1].

The samples were synthesized as stabilized sols of the corresponding metal hydroxides. The synthesis procedures consisted of the following steps: (i) forced hydrolysis of an inorganic metal

* Corresponding author. Tel.: +375 172008106; fax: +375 172264696.
*E-mail addresses:* ivanovskaya@bsu.by (M.I. Ivanovskaya), pietro.siciliano@le.imm.cnr.it (P. Siciliano).

0925-4005/$ – see front matter © 2007 Elsevier B.V. All rights reserved.
doi:10.1016/j.snb.2006.12.011

salt solution (0.5 mol $l^{-1}$) with a base agent (water solution of $NH_3$, >99.99% purity, 0.5 mol $l^{-1}$); (ii) precipitation of a metal hydroxide and its separation from the liquid phase; (iii) formation of a sol by peptization of the deposit with peptizing agent ($HNO_3$) or as a result of self-peptization.

$Fe(NO_3)_3{\cdot}9H_2O$, $FeSO_4$ and $In(NO_3)_3{\cdot}4.5H_2O$ salts, all with stated purities >99.9%, were used as inorganic precursors for iron and indium oxides, respectively, both in simple and composite systems.

Single **$In_2O_3$** and **α-$Fe_2O_3$** samples were synthesized by hydrolysis of In(III) and Fe(III) salts, respectively. The sols were obtained as a result of self-peptization of the corresponding metal hydroxides.

Single **γ-$Fe_2O_3$** sol was obtained by oxidation of $Fe_3O_4$ sol at 100 °C for 5 h by an intense flow of air. The sol of $Fe_3O_4$ was prepared by combined hydrolysis of Fe(III) and Fe(II) salts (Fe(III):Fe(II) = 2:1 mol) with subsequent peptization.

The formation of $Fe_2O_3$–$In_2O_3$ sample based on α-$Fe_2O_3$ (**α-$Fe_2O_3$–$In_2O_3$** sample) was achieved by combined hydrolysis of Fe(III) and In(III) salts.

**I-γ-$Fe_2O_3$–$In_2O_3$** sample was prepared by simultaneous hydrolysis of In(III), Fe(III) and Fe(II) salts, and subsequent oxidation of the product.

An alternative way to obtain the $Fe_2O_3$–$In_2O_3$ system containing γ-$Fe_2O_3$ phase was attained by mixing the preliminary prepared individual **$In_2O_3$** and **γ-$Fe_2O_3$** sols (**II-γ-$Fe_2O_3$–$In_2O_3$** sample).

Table 1 summarizes the synthesis conditions under which the above-mentioned oxides were obtained.

The structure of the samples was characterized by means of X-ray diffraction (XRD) analysis, high-resolution transmission electron microscopy (TEM), electron diffraction (ED), Mössbauer spectroscopy, and differential thermal analysis and thermogravimetry (DTA/TG). XRD analysis was carried out on a *HZG-4A* diffractometer by using Co Kα radiation. TEM/ED examinations were performed with a *LEO 906E* and a *JEOL 4000 EX* high-resolution transmission electron microscopes. The resonance spectra were recorded in air at 298 K and processed by using a commercial SM2201 Mössbauer spectrometer equipped with a 15 mCi $^{57}Co$ (Rh) source. Simultaneous DTA and TG analyses were carried out on an *OD-102* instrument in air with a 5 °C $min^{-1}$ heating rate.

In order to obtain thin-film sensors, the sols were deposited by spin-coating onto special polycrystalline $Al_2O_3$ substrates (3 mm × 3 mm × 0.25 mm) supplied with Pt interdigitated electrode structure on the front side and a Pt-heater on the rear side. The thickness of the thin films was estimated to be about 200 nm. The sensor elements were successively annealed at 300–400 °C for 96 h in air. A further thermal treatment up to 500–800 °C was performed in order to characterize the crystallization process of the $Fe_2O_3$–$In_2O_3$ composites. The gas-sensing responses of the films to $C_2H_5OH$ and $NO_2$ gases were studied and correlated with the structural properties of the active materials. Contact electric potential was applied to the interdigitated electrode structure and current through a sensing layer in air and in air–gas mixtures was measured. The response (*S*) of the sensors was calculated as $I_{air}/I_{gas}$ and $I_{gas}/I_{air}$ when detecting oxidizing ($NO_2$) and reducing ($C_2H_5OH$) gases, respectively. The measurements were performed in a flow chamber (0.2 l) at 0.3 l $min^{-1}$ flow rate, 20 °C temperature and 30% relative humidity.

Table 1
Synthesis conditions of the samples studied in the paper

| Sample designation | Synthesis conditions |
|---|---|
| **$In_2O_3$** | Introduction of $NH_3$ solution into $In(NO_3)_3$ solution |
| **γ-$Fe_2O_3$** | Introduction of $Fe(NO_3)_3$–$FeSO_4$ (2:1 mol) solution into $NH_3$ solution and oxidation of the suspension with air (5 h, 100 °C) |
| **α-$Fe_2O_3$** | Introduction of $NH_3$ solution into $Fe(NO_3)_3$ solution |
| **α-$Fe_2O_3$–$In_2O_3$ (9:1)** | Introduction of $NH_3$ solution into $Fe(NO_3)_3$–$In(NO_3)_3$ (9:1 mol) solution |
| **I-γ-$Fe_2O_3$–$In_2O_3$ (9:1)** | Introduction of $Fe(NO_3)_3$–$FeSO_4$–$In(NO_3)_3$ (9:4.5:0.75 mol) solution into $NH_3$ solution and oxidation of the suspension with air (5 h, 100 °C) |
| **II-γ-$Fe_2O_3$–$In_2O_3$ (9:1)** | Mixing of **γ-$Fe_2O_3$** and **$In_2O_3$** (9:1 mol) sols |

## 3. Results and discussion

### 3.1. System α-$Fe_2O_3$–$In_2O_3$

The **α-$Fe_2O_3$–$In_2O_3$** composite, obtained by combined hydrolysis of $Fe(NO_3)_3$ and $In(NO_3)_3$ salts and subsequent co-precipitation of the resulting Fe(III) and In(III) hydroxides, remains X-ray amorphous after its thermal treatment at 150–300 °C (Fig. 1). After annealing the composite at 500 °C, broadened reflections of the α-$Fe_2O_3$ phase (*ref.* JCPDS 33-0664) appear in the XRD pattern.

The increase of the experimental lattice parameters compared to the reference data for α-$Fe_2O_3$ phase, as well as the absence of reflexes deriving from indium-oxide phases, can be explained by

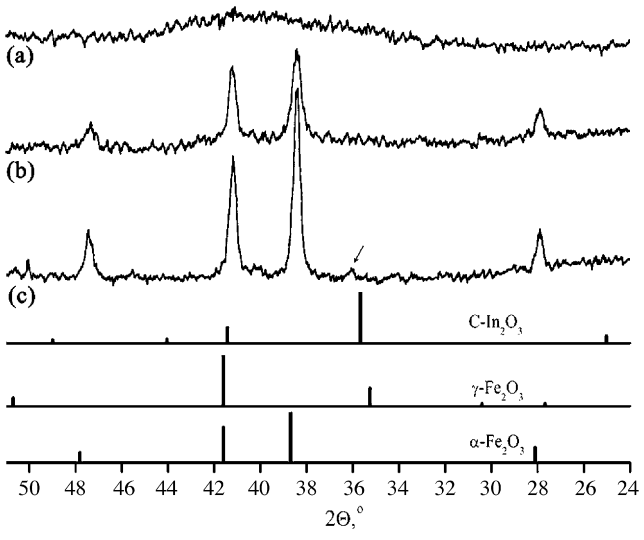


Fig. 1. XRD patterns of the **α-$Fe_2O_3$–$In_2O_3$** sample annealed at different temperatures: (a) 300 °C; (b) 500 °C; (c) 800 °C.

Table 2
Comparison between the experimental interplanar spacings derived from the ED pattern in Fig. 2c and the theoretical values of the α-$Fe_2O_3$ phase

| Line number | $d_{measured}$ (Å) | α-$Fe_2O_3$ (JCPDS 33-0664) | | |
|---|---|---|---|---|
| | | $d_{calculated}$ (Å) | $I$ (%) | $h\,k\,l$ |
| 1 | 3.71 | 3.68 | 30 | 0 1 2 |
| 2 | 2.70 | 2.70 | 100 | 1 0 4 |
| 3 | 2.52 | 2.52 | 70 | 1 1 0 |
| 4 | 2.22 | 2.21 | 20 | 1 1 3 |
| 5 | 1.85 | 1.84 | 40 | 0 2 4 |
| 6 | 1.70 | 1.69 | 45 | 1 1 6 |
| 7 | 1.60 | 1.60 | 10 | 0 1 8 |
| 8 | 1.50 | 1.48 | 30 | 2 1 4 |
| 9 | 1.46 | 1.45 | 30 | 3 0 0 |

the formation of an α-$Fe_{2-x}In_xO_3$ solid solution, incorporating the total amount of indium within the α-$Fe_2O_3$ lattice. A high mutual solubility of α-$Fe_2O_3$ and $In_2O_3$ oxides at 600 °C has been reported in a previous work [5]. A noticeable destruction of the α-$Fe_{2-x}In_xO_3$ solid solution and isolation of individual C-$In_2O_3$ phase (*ref.* JCPDS 39-1346) start at 800 °C since its main diffraction reflection (marked with an arrow) can be distinguished in the corresponding XRD pattern. The shift of the reflection toward greater angle values (i.e. decrease of lattice parameters) is the evidence of substitution of indium ions by smaller iron ions in the $In_2O_3$ crystal lattice. A more detailed analysis of the fine structure of the **α-$Fe_2O_3$–$In_2O_3$** composite annealed at 300 °C (not allowed by the XRD) was obtained by TEM/ED characterization. As shown by the images in Fig. 2a and b, the X-ray amorphous **α-$Fe_2O_3$–$In_2O_3$** composite consists of small ($d \leq 10$ nm) near spherical grains. The ED pattern of this composite is reported in Fig. 2c.

The ED data presented in Table 2 demonstrate that α-$Fe_2O_3$ with hexagonal structure forms at the annealing temperature of 300 °C.

The Mössbauer spectrum of such a sample, reported in Fig. 3a, shows a paramagnetic doublet. The lack of a magnetic order ($B = 0$) in the sample arises from its high dispersity. The occurrence of $In^{3+}$ ions within the α-$Fe_2O_3$ crystalline lattice is likely to produce a distortion of the $Fe^{3+}$ coordination environment symmetry and leads to an increased quadrupole splitting parameter ($\Delta$), as compared to the value typical of the individual α-$Fe_2O_3$ oxide (Table 3) [8].

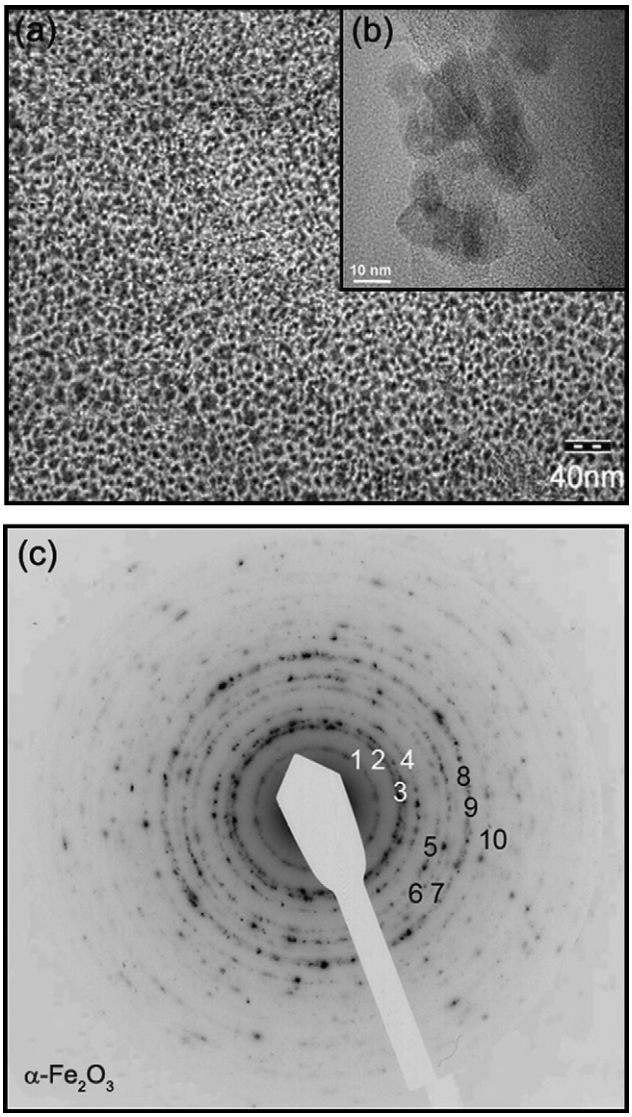


Fig. 2. TEM images (a and b) and ED pattern (c) of the **α-$Fe_2O_3$–$In_2O_3$** sample annealed at 300 °C.

### 3.2. System γ-$Fe_2O_3$–$In_2O_3$

The formation of the **γ-$Fe_2O_3$–$In_2O_3$** composite is related to the synthesis of the thermodynamically metastable γ-$Fe_2O_3$ phase. One of the approaches assumes the formation of γ-$Fe_2O_3$

Table 3
Parameters of the $^{57}$Fe Mössbauer spectra recorded form the **$Fe_2O_3$–$In_2O_3$** composites and individual iron oxides annealed at 300 °C

| Sample | $\delta$ (±0.03; mm/s) | $\Delta$ (±0.03; mm/s) | $B$ (±0.5; T) | $W$ (±5; %) | Phase |
|---|---|---|---|---|---|
| **α-$Fe_2O_3$–$In_2O_3$ (9:1)** ($Fe^{3+}$/$In^{3+}$ co-precipitation) | 0.30 | 0.78 | 0 | 100 | α-$Fe_{2-x}In_xO_3$ |
| **I-γ-$Fe_2O_3$–$In_2O_3$ (9:1)** ($Fe^{3+}$/$Fe^{2+}$/$In^{3+}$ co-precipitation) | 0.38 | 0.08 | 50.5 | 75 | Q-γ-$Fe_2O_3$ |
| | 0.53 | 0 | 0 | 15 | C-γ-$Fe_2O_3$ |
| | 0.22 | 0.69 | 0 | 10 | α-$Fe_{2-x}In_xO_3$ |
| **II-γ-$Fe_2O_3$–$In_2O_3$ (9:1)** (γ-$Fe_2O_3$/$In_2O_3$ mixing) | 0.33 | 0.02 | 48.5 | 100 | γ-$Fe_2O_3$ |
| **γ-$Fe_2O_3$** | 0.34 | −0.03 | 49.0 | 100 | γ-$Fe_2O_3$ |
| **α-$Fe_2O_3$** | 0.39 | 0.09 | 50.7 | 100 | α-$Fe_2O_3$ |
| γ-$Fe_2O_3$ (reference) [9] | 0.34 | −0.05 | 49.8 | 100 | γ-$Fe_2O_3$ |
| α-$Fe_2O_3$ (reference) [9] | 0.38 | 0.12 | 51.5 | 100 | α-$Fe_2O_3$ |

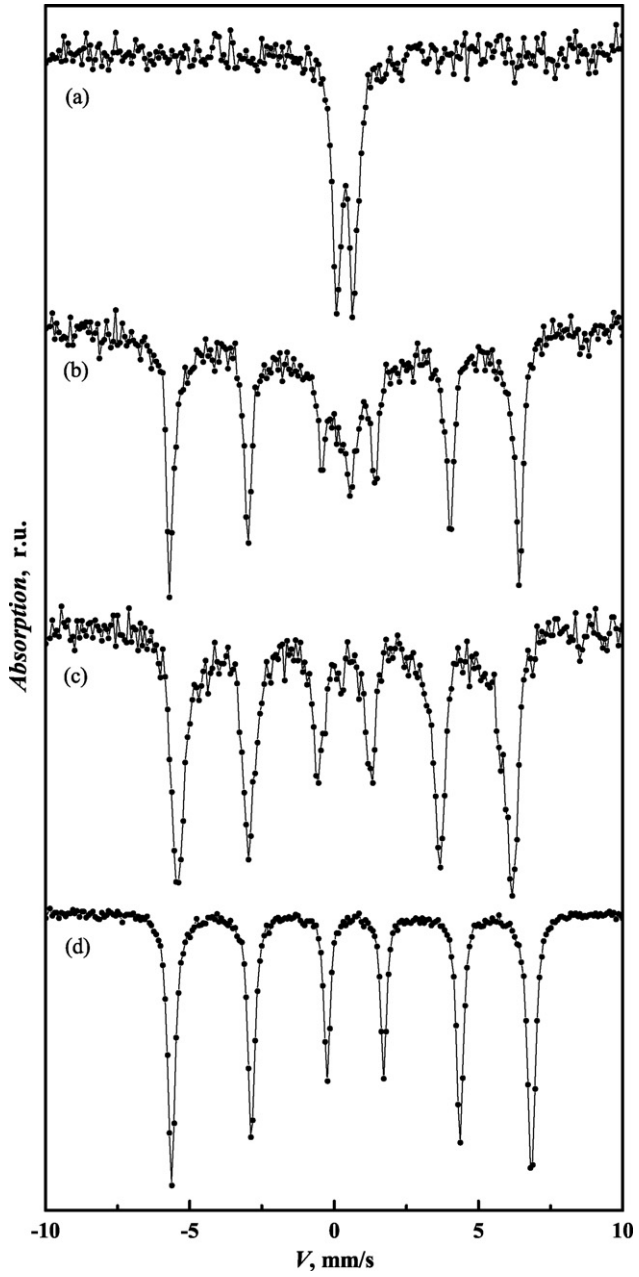


Fig. 3. $^{57}$Fe Mössbauer spectra recorded from the samples annealed at 300 °C: (a) **α-$Fe_2O_3$–$In_2O_3$ (9:1)**; (b) **I-γ-$Fe_2O_3$–$In_2O_3$ (9:1)**; (c) **II-γ-$Fe_2O_3$–$In_2O_3$ (9:1)**; (d) α-$Fe_2O_3$ (reference).

via magnetite ($Fe_3O_4$) intermediate. Magnetite has a structure, which is close to the structure of cubic γ-$Fe_2O_3$, differing from it in the absence of vacancies in the cationic sub-lattice. Thus, γ-$Fe_2O_3$ phase can be obtained by oxidation of $Fe_3O_4$ under controlled conditions [9,10].

The previous considerations allow to assume that the $Fe_2O_3$–$In_2O_3$ composite based on γ-$Fe_2O_3$ phase can be obtained by simultaneous hydrolysis of In(III), Fe(III) and Fe(II) salts, and subsequent oxidation of the product. However, competitive processes, such as formation of α-$Fe_2O_3$ and $In_2O_3$ phases, are possible under the indicated conditions. Moreover, the rates of hydrolysis of Fe(III) and Fe(II) salts are known to differ substantially [11,12]. Therefore, products of complicated phase composition can be expected [13].

Table 4
Comparison between the experimental interplanar spacings derived from the ED pattern in Fig. 5d and the theoretical values of the α-$Fe_2O_3$ phase

| Line number | $d_{measured}$ (Å) | α-$Fe_2O_3$ (JCPDS 33-0664) | | |
|---|---|---|---|---|
| | | $d_{calculated}$ (Å) | $I$ (%) | $hkl$ |
| 1 | 2.71–2.53 | 2.70 | 100 | 1 0 4 |
| | | 2.52 | 70 | 1 1 0 |
| 2 | 2.46–2.16 | 2.20 | 20 | 1 1 3 |
| 3 | 1.58–1.50 | 1.60 | 5 | 1 2 2 |
| | | 1.60 | 10 | 0 1 8 |
| | | 1.48 | 30 | 2 1 4 |
| 4 | 1.29–1.18 | 1.31 | 10 | 1 0 1 0 |
| | | 1.19 | 5 | 1 2 8 |

The experimental X-ray data showed that the **I-γ-$Fe_2O_3$–$In_2O_3$** composite obtained under the above indicated synthesis conditions is amorphous for an annealing temperature of 150 °C. A crystalline structure appears after annealing at 300 °C, as visible in the relevant diffraction pattern reported in Fig. 4. It shows inhomogeneously broadened asymmetric reflections, which can be ascribed mainly to hexagonal α-$Fe_2O_3$ phase, as well as, in minor measure, to both cubic (C-γ-$Fe_2O_3$) (*ref.* JCPDS 39-1346) and tetragonal (Q-γ-$Fe_2O_3$) (*ref.* JCPDS 25-1402, 13-0458) modifications of γ-$Fe_2O_3$.

This could be better evidenced by TEM and ED investigations, which confirmed the presence of anisotropic particles of Q-γ-$Fe_2O_3$ in the considered **I-γ-$Fe_2O_3$–$In_2O_3$** sample (Fig. 5). In particular, the sample is composed of two types of particles, which differ substantially in size and morphology. Fig. 5b shows highly dispersive ($d \sim 5$ nm) spherical grains whose ED pattern is typical of α-$Fe_2O_3$ phase (Table 4). The second type of grains has a plate-like shape and a size of about 10 nm × 30 nm. The analysis of the ED pattern obtained from such grains (Fig. 5e) reveals the presence of γ-$Fe_2O_3$ phase (Table 5); as the lattice parameters of C-γ-$Fe_2O_3$ ($a = 0.8340$ nm; symmetry group *Fdm*) and Q-γ-$Fe_2O_3$ ($a = 0.8338$ nm, $c/3 = 0.8322$ nm; symmetry group $P4_132$) are very similar, it is not possible to distinguish precisely between cubic and tetragonal modifications; nevertheless, the presence of both is expected, with a prevalence of the tetragonal one (*ref.* JCPD 25-1402), since the formation of the tetragonal γ-$Fe_2O_3$ phase is considered as perfecting the crystalline structure of C-γ-$Fe_2O_3$, during the annealing and crystal growth [10,14–16]. In particular, the degree of ordering of the cation vacancies increases, leading to the formation of a superstructure, peculiar to the tetragonal γ-$Fe_2O_3$ lattice cell but not to the cubic one (Fig. 6), where cation vacancies are distributed statistically between the octahedral interstices.

The electron diffraction gives also indications about the anisotropy of the Q-γ-$Fe_2O_3$ particles, as only high order *l*-index reflections appear (2 0 6, 1 1 9, 2 0 9, 3 1 6, 0 0 12, 2 1 12, 2 0 15, 3 3 1 5, 2 2 24). These results are in agreement with the XRD data and confirm the anisotropic growth of the Q-γ-$Fe_2O_3$ crystals along the [0 0 1] orientation, which coincides with the

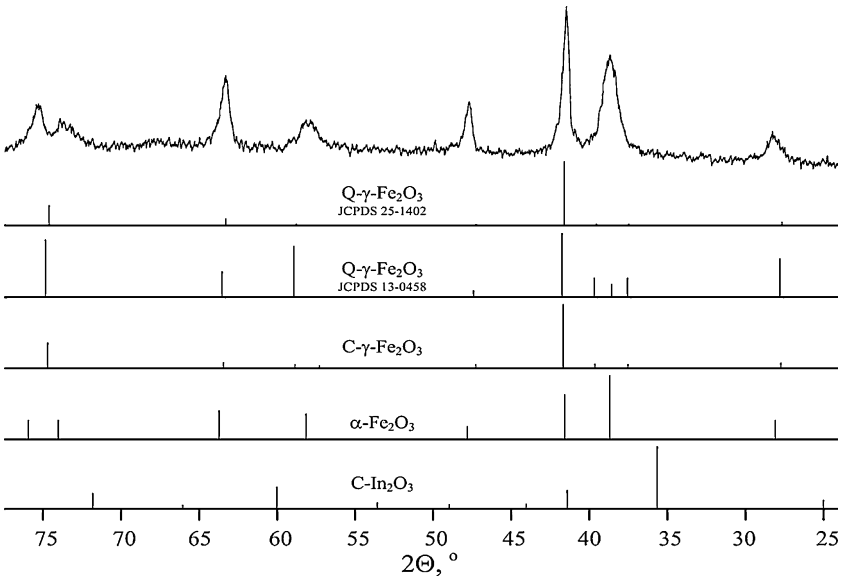


Fig. 4. XRD pattern of the **I-γ-$Fe_2O_3$–$In_2O_3$ (9:1)** composite annealed at 300 °C and stroke patterns of the reference phases.

vector of light magnetization in γ-$Fe_2O_3$ structure. The magnetic crystallographic anisotropy of γ-$Fe_2O_3$ favors both the anisotropic crystal growth and the formation of the tetragonal structure of γ-$Fe_2O_3$ lattice. No reflections due to any indium oxide phases were detected in the considered ED pattern. The absence of separate indium oxide phases in this sample was also confirmed by Mössbauer examination as described below.

An intricate Mössbauer spectrum of the **I-γ-$Fe_2O_3$–$In_2O_3$** sample (see Fig. 3b) reflects the complex phase composition of the oxide system obtained as a result of simultaneous hydrolysis of In(III), Fe(III) and Fe(II) salts. The results of the spectrum splitting ($\delta$, $\Delta$, $B$ parameters) and phase compositions are listed in Table 3 and allow to infer the following conclusions: most of the $Fe^{3+}$ ions (∼75%) have symmetry of coordination environment slightly different from cubic. This is typical of Q-γ-$Fe_2O_3$ structure. About 15% of the $Fe^{3+}$ ions have parameters very close to those of C-γ-$Fe_2O_3$. Coordination symmetry of a minor part of the $Fe^{3+}$ ions (∼10%) differs substantially from cubic and can be the result of substitutional α-$Fe_{2-x}In_xO_3$ solid solution formation. The lack of magnetic ordering in the last two phases – C-γ-$Fe_2O_3$ and α-$Fe_{2-x}In_xO_3$ – is caused by the small size of the grains. No $Fe^{2+}$ ions, which were initially introduced into the reaction media, were detected in the target product. These conclusions are in good agreement with the structural results of the TEM analysis.

Table 5
Comparison between the experimental interplanar spacings derived from the ED pattern in Fig. 5e and the theoretical values of the C-γ-$Fe_2O_3$ and Q-γ-$Fe_2O_3$ phases

| Line number | $d_{measured}$ (Å) | C-γ-$Fe_2O_3$ (JCPDS 39-1346) | | | Q-γ-$Fe_2O_3$ (JCPDS 25-1402) | | |
|---|---|---|---|---|---|---|---|
| | | $d_{calculated}$ (Å) | $I$ (%) | $hkl$ | $d_{calculated}$ (Å) | $I$ (%) | $hkl$ |
| 1 | 2.99 | 2.95 | 35 | 2 2 0 | 2.95 | 30 | 2 0 6 |
| 2 | 2.46 | 2.52 | 100 | 3 1 1 | 2.51 | 100 | 1 1 9 |
| 1[a] | 2.33 | 2.32 | 1 | 3 2 0 | 2.32 | 2 | 2 0 9 |
| 2[a] | 2.24 | 2.23 | 1 | 3 2 1 | 2.23 | 2 | 3 1 6 |
| 3 | 2.12–2.05 | 2.09 | 16 | 4 0 0 | 2.09 | 15 | 0 0 12 |
| 4 | 1.83–1.79 | 1.82 | 2 | 4 2 1 | 1.82 | 3 | 2 1 12 |
| 3[a] | 1.56 | 1.55 | 1 | 5 2 0 | 1.55 | 2 | 2 0 15 |
| 5 | 1.51 | 1.48 | 34 | 4 4 0 | 1.52 | 3 | 2 1 15 |
| 4[a] | 1.40 | 1.39 | 1 | 4 4 2 | – | – | – |
| 6 | 1.28 | – | – | – | 1.27 | 8 | 3 3 15 |
| 5[a] | 1.23 | 1.23 | 1 | 6 3 1 | – | – | – |
| 6[a] | 1.15 | 1.14 | 1 | 7 2 1 | – | – | – |
| 7 | 1.09 | 1.09 | 7 | 7 3 1 | 1.09 | 10 | 2 1 21 |
| 8 | 1.05 | 1.04 | 3 | 8 0 0 | 1.04 | 7 | 0 0 24 |
| 7[a] | 0.97 | [b] | [b] | [b] | 0.98 | 5 | 2 2 24 |
| 9 | 0.90 | [b] | [b] | [b] | [b] | [b] | [b] |
| 10 | 0.83 | [b] | [b] | [b] | [b] | [b] | [b] |
| 11 | 0.81 | [b] | [b] | [b] | [b] | [b] | [b] |

[a] Spot reflection.
[b] The data are absent.

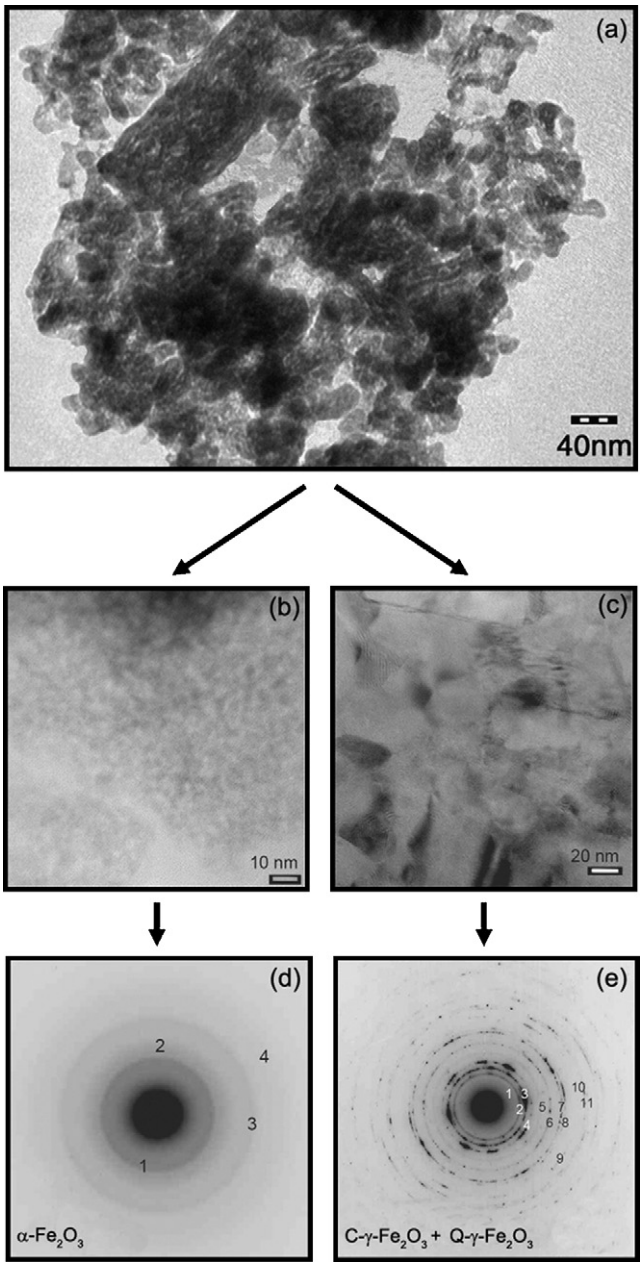


Fig. 5. TEM images (a–c) and ED patterns (d and e) of the **I-γ-$Fe_2O_3$–$In_2O_3$ (9:1)** sample annealed at 300 °C.

A TEM image of the **II-γ-$Fe_2O_3$–$In_2O_3$** sample, obtained by mixing the preliminary prepared individual **$In_2O_3$** and **γ-$Fe_2O_3$** sols and annealed at 300 °C, is given in Fig. 7. The sample consists of spherical grains with a diameter of 4–8 nm. XRD examination of the composite annealed at 150 °C shows the presence of the C-γ-$Fe_2O_3$ crystalline phase (Fig. 8). One weak (2 0 0)-reflection of InOOH phase is also present in the pattern. The increase of the annealing temperature to 300–400 °C causes the formation of the C-γ-$Fe_2O_3$ and C-$In_2O_3$ crystalline phases, whose experimental lattice parameters are in very good agreement with the reference data. According to DTA data, the thermo-stimulated γ-$Fe_2O_3$ → α-$Fe_2O_3$ transformation occurs in the considered **II-γ-$Fe_2O_3$–$In_2O_3$** composite at 455 °C that slightly exceeds the temperature of the same transformation in the individual **γ-$Fe_2O_3$** oxide (435 °C).

The obtained results give evidence that mixing individual sols of $In_2O_3 \cdot nH_2O$ and γ-$Fe_2O_3 \cdot nH_2O$ prevents oxide phases from mutual doping at the stage of their crystallization. The observed phenomenon can be connected with the specificity of the γ-$Fe_2O_3 \cdot nH_2O$ sol synthesis. It includes a stage of long-term (5 h) oxidation of $Fe_3O_4 \cdot nH_2O$ sol at rather high temperature (100 °C) that promotes both crystallization processes and particle growth. The lack of mutual doping in the considered composite was also confirmed by Mössbauer spectroscopy examination. Therefore, the spectrum parameters of the sample annealed at 300 °C are close to the parameters of the highly dispersed individual **γ-$Fe_2O_3$** sample (see Fig. 3; Table 3). However, the presence of indium in the **II-γ-$Fe_2O_3$–$In_2O_3$** composite influences grain size of the C-γ-$Fe_2O_3$ phase since the $In_2O_3$ grains seem to hamper the C-γ-$Fe_2O_3$ grain growth during the crystallization process.

Table 6 summarizes the results of various structural examinations of the **$Fe_2O_3$–$In_2O_3$ (9:1)** samples obtained under various synthesis conditions.

### *3.3. Gas-sensing features of the $Fe_2O_3$–$In_2O_3$ thin-film sensors*

The thin-film sensors based on the obtained individual oxides ($In_2O_3$, α-$Fe_2O_3$, γ-$Fe_2O_3$), as well as on the $Fe_2O_3$–$In_2O_3$ composites with different structure, were tested to $C_2H_5OH$ vapors and $NO_2$. Table 7 compares the maximum response values and optimal operating temperatures of the sensors. The corresponding signal profiles for the composites are given in Figs. 9 and 10. The α-$Fe_2O_3$-based sensor and especially

Table 6
Phase composition and grain size of the **$Fe_2O_3$–$In_2O_3$ (9:1)** samples studied in the paper

| Composite | Synthesis conditions | Phase composition | *d* (nm) |
|---|---|---|---|
| **I-α-$Fe_2O_3$–$In_2O_3$** | Co-precipitation, $Fe^{3+}/In^{3+}$ | α-$Fe_{2-x}In_xO_3$ | 3–10 |
| **I-γ-$Fe_2O_3$–$In_2O_3$** | Co-precipitation, $Fe^{2+}/Fe^{3+}/In^{3+}$ | α-$Fe_{2-x}In_xO_3$ | ∼5 |
| | | Q-γ-$Fe_2O_3$ | 10 × 30 |
| | | C-γ-$Fe_2O_3$ | – |
| **II-γ-$Fe_2O_3$–$In_2O_3$** | Mixing, **γ-$Fe_2O_3$/$In_2O_3$** | γ-$Fe_2O_3$ | 4–8 |
| | | C-$In_2O_3$ | |

Annealing temperature is 300 °C.

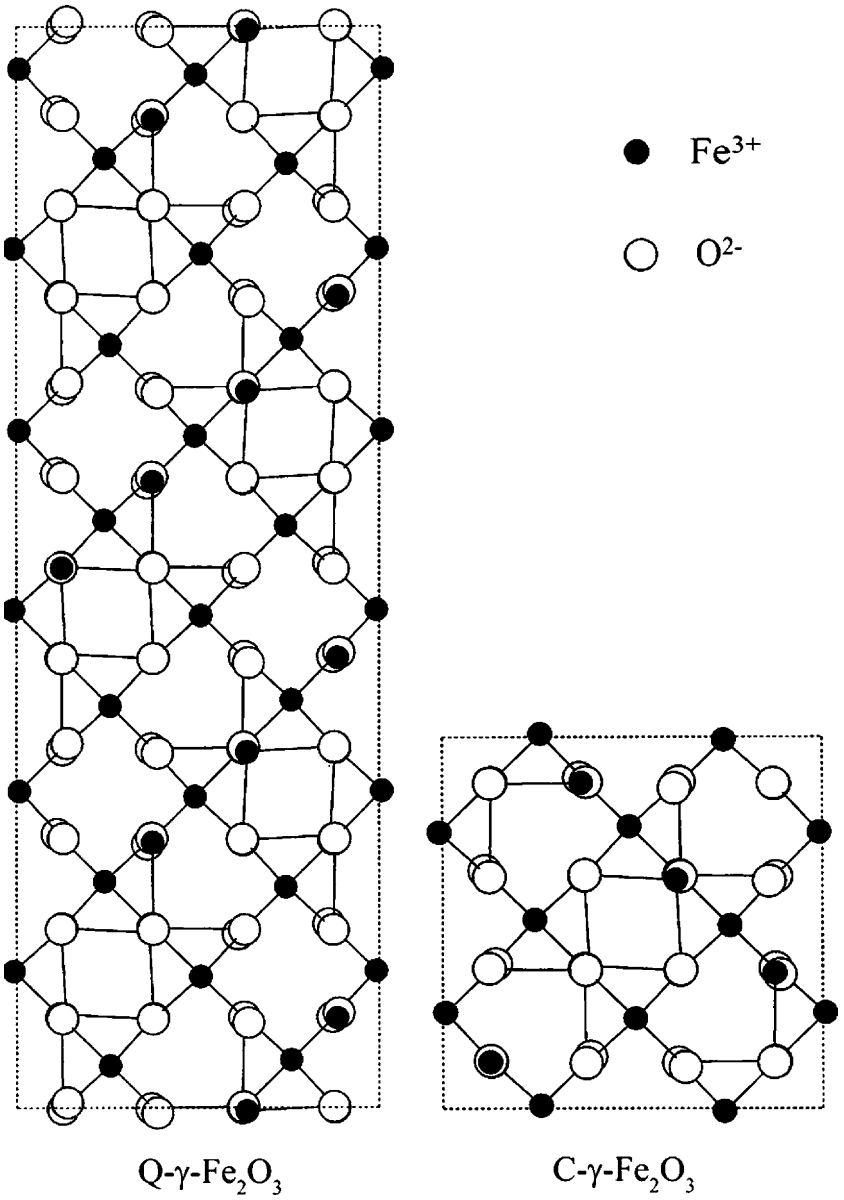


Fig. 6. Schematic representation of tetragonal (Q-) and cubic (C-) γ-$Fe_2O_3$ lattices, [0 1 0]-view.

Table 7
Phase composition of various oxide systems and gas-sensing features of the corresponding thin-film sensors regarding $C_2H_5OH$ vapors and $NO_2$

| Sensing layer | Phase composition | $C_2H_5OH$ (50 ppm) | | $NO_2$ (0.5 ppm) | |
|---|---|---|---|---|---|
| | | *S* (r.u.) | *t* (°C) | *S* (r.u.) | *t* (°C) |
| **α-$Fe_2O_3$–$In_2O_3$ (9:1)** | α-$Fe_{2-x}In_xO_3$ | 2 | 250 | 1.5 | 135 |
| **I-γ-$Fe_2O_3$–$In_2O_3$ (9:1)** | Q-γ-$Fe_2O_3$<br>C-γ-$Fe_2O_3$<br>α-$Fe_{2-x}In_xO_3$ | 27 | 250 | 75 | 135 |
| **II-γ-$Fe_2O_3$–$In_2O_3$ (9:1)** | C-γ-$Fe_2O_3$<br>C-$In_2O_3$ | 25 | 350 | 65 | 135 |
| **$In_2O_3$** | C-$In_2O_3$ | 15 | 350 | 35 | 150 |
| **α-$Fe_2O_3$** | α-$Fe_2O_3$ | 9 | 250 | 1.5 | 200 |
| **γ-$Fe_2O_3$** | γ-$Fe_2O_3$ | 15 | 300 | 5 | 200 |

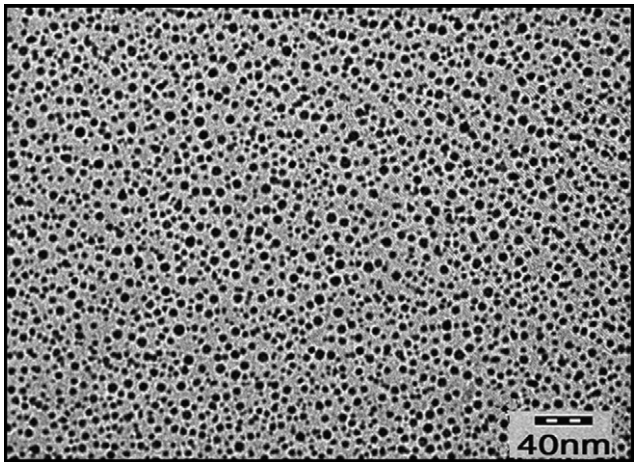


Fig. 7. TEM image of the **II-γ-$Fe_2O_3$–$In_2O_3$ (9:1)** sample annealed at 300 °C.

the **α-$Fe_2O_3$–$In_2O_3$** sensor show the lowest response values to both $C_2H_5OH$ and $NO_2$. This result is expected since α-$Fe_2O_3$ phase is the most stable modification of iron oxide; therefore it should be less active in various electrophysical processes that cause a semiconductor sensor response. The poor performance of the **α-$Fe_2O_3$–$In_2O_3$** layer, which is formed of super fine particles of a single-phase α-$Fe_{2-x}In_xO_3$ solid solution, could be attributed both to its structural similarity to the α-$Fe_2O_3$-based sensor and to its extremely high resistance, which lower the sensitivity to the gas species [1].

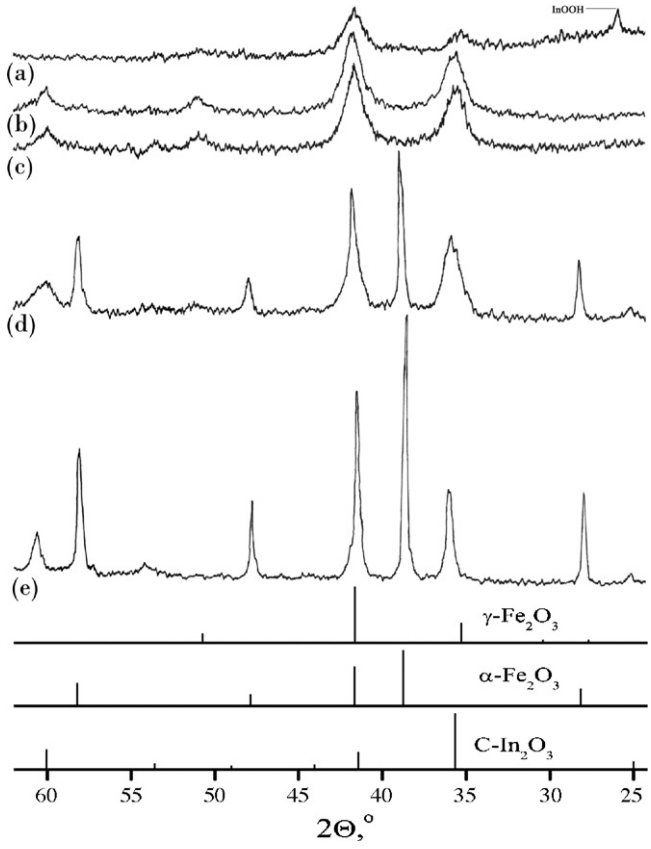


Fig. 8. XRD pattern of the **II-γ-$Fe_2O_3$–$In_2O_3$ (9:1)** composite annealed at different temperatures: (a) 150 °C; (b) 300 °C; (c) 400 °C; (d) 500 °C; (e) 800 °C.

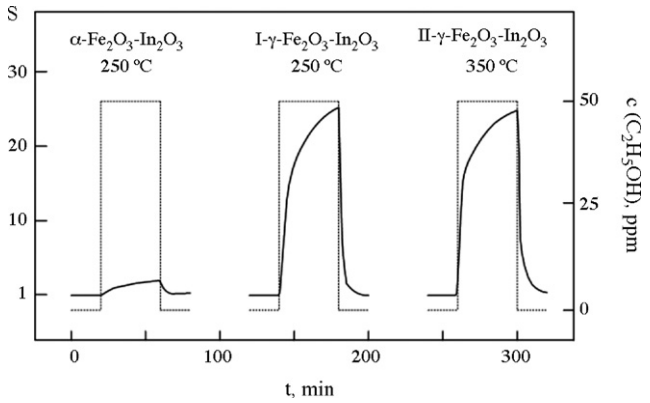


Fig. 9. Response curves of different **$Fe_2O_3$–$In_2O_3$** sensors to $C_2H_5OH$ at optimal operating temperatures.

Individual **γ-$Fe_2O_3$** thin film, which is composed of γ-$Fe_2O_3$ phase, demonstrates higher response values to $C_2H_5OH$ and $NO_2$ as compared to α-$Fe_2O_3$-based layers. The higher activity of the γ-$Fe_2O_3$ phase is associated with the specificity of its structure, its metastability, the presence of metal cation vacancies in crystalline lattice and the readiness of $Fe^{2+} \leftrightarrow Fe^{3+}$ transformation upon exposure to gas media [4–7]. Besides, partial reversible reduction of a γ-$Fe_2O_3$-based material by $C_2H_5OH$ to form α-$Fe_2O_3$ phase is possible. The product of reduction is highly dispersive and strongly reactive and resembles the behavior of γ-$Fe_2O_3$ [1,7].

The **II-γ-$Fe_2O_3$–$In_2O_3$** thin-film sensor exceeds the sensitivity of the sensors based on individual γ-$Fe_2O_3$ oxide. This is related to the presence in the **II-γ-$Fe_2O_3$–$In_2O_3$** composite of two highly dispersed phases: γ-$Fe_2O_3$ and $In_2O_3$. The heterojunction between these phases appears to be active in both adsorption and chemical transformation of $C_2H_5OH$ and $NO_2$. The presence of two types of adsorption centers, having different reductive–oxidative and acid–base properties, and participating in the processes of the alcohol molecule transformation, is an essential requirement to achieve high sensor response when alcohol detection is considered. The centers of one type can suitably participate in adsorption–desorption processes of alcohol molecules, whereas complete oxidation effectively proceeds at

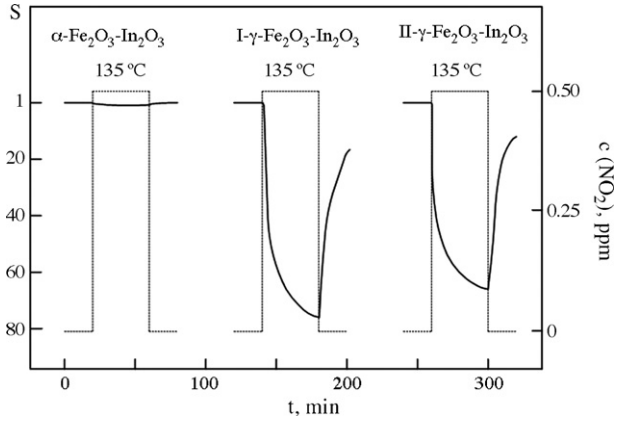


Fig. 10. Response curves of different **$Fe_2O_3$–$In_2O_3$** sensors to $NO_2$ at optimal operating temperatures.

the centers of the other type [1,17–19]. The most essential difference in sensitivity of the **γ-$Fe_2O_3$** and **II-γ-$Fe_2O_3$–$In_2O_3$** layers could be noted under detection of $NO_2$. In the case of $NO_2$ detection, high defectiveness of oxide materials is the most critical requirement to achieve great response values [20].

As can be seen form the Table 7 and Figs. 9 and 10, the **I-γ-$Fe_2O_3$–$In_2O_3$** sensor demonstrates the greatest sensitivity among the studied materials. As opposed to **II-γ-$Fe_2O_3$–$In_2O_3$**, this composite includes three phases: α-$Fe_{2-x}In_xO_3$ solid solution, cubic γ-$Fe_2O_3$ and tetragonal γ-$Fe_2O_3$ with a superstructure of cationic vacancies. The developed interfacial areas between the indicated nanosized phases result in better sensing performance.

Both the **I-γ-$Fe_2O_3$–$In_2O_3$** and **II-γ-$Fe_2O_3$–$In_2O_3$** thin films excel substantially in sensitivity the sensors based on individual $In_2O_3$ and γ-$Fe_2O_3$ oxides, as well as earlier sensors based on $In_2O_3$–$MoO_3$ [20], $In_2O_3$–NiO [21] and $SnO_2$–$MoO_3$ [22] composites. It is worth noting that in contrast to the individual **γ-$Fe_2O_3$** layer, the **II-γ-$Fe_2O_3$–$In_2O_3$** thin-film sensors appear to be more stable and selective to $C_2H_5OH$ vapors in the presence of CO, $CH_4$, $NO_2$ and $O_3$, as already demonstrated in [1].

Thus, high performances of the considered **γ-$Fe_2O_3$–$In_2O_3$** gas-sensing layers were achieved by an optimal combination of grain size, surface activity, nature and amount of adsorption and catalytic centers. Moreover, the obtained results show that the more complex the structure of the $Fe_2O_3$–$In_2O_3$ composite the greater its response to gases of various chemical nature-oxidants ($NO_2$) and reductants ($C_2H_5OH$). As a matter of fact, the presence of adsorption centers of different nature on the surface of the complex $Fe_2O_3$–$In_2O_3$ gas-sensing materials creates the necessary prerequisites for multi-route activation of various reactions during the detection process.

## 4. Conclusion

The influence of synthesis conditions on the structural and gas-sensing properties of $Fe_2O_3$–$In_2O_3$ composites has been carefully analyzed. It was found that co-precipitation of Fe(III) and In(III) hydroxides leads to the formation of an α-$Fe_{2-x}In_xO_3$ single-phase solid solution, which is homogeneous and poorly crystalline. The thermodynamic stability of this phase along with high structural homogeneity of the sample causes its poor sensitivity to both reducing and oxidizing gases.

The heterogeneous $Fe_2O_3$–$In_2O_3$ composite based on cubic $In_2O_3$ and metastable γ-$Fe_2O_3$ phases was obtained by mixing the individual sols of hydrated $In_2O_3$ and γ-$Fe_2O_3$ oxides. It demonstrates much greater response values due to high activity of metastable γ-$Fe_2O_3$ structure in adsorption and electrophysical processes.

Simultaneous precipitation of Fe(III) and Fe(II) hydroxides in the presence of In(III) salt results in a multi-phase product consisting of α-$Fe_{2-x}In_xO_3$ solid solution, cubic γ-$Fe_2O_3$ and tetragonal γ-$Fe_2O_3$ phase with a superstructure of cationic vacancies. This structure provides substantial improvement of gas sensor performances in comparison with the homogeneous α-$Fe_2O_3$–$In_2O_3$ composites. As general conclusion it can be stated that the complexity of the oxide-based systems that appears as a stabilization of new phases and formation of structurally inhomogeneous nanosized heterojunction composites, gives new possibilities in the development of advanced gas sensors for detection of various gaseous species.

## Acknowledgement

D. Kotsikau thanks the Belarusian Foundation of Fundamental Investigations for financial support.

## References

[1] M. Ivanovskaya, D. Kotsikau, G. Faglia, P. Nelli, S. Irkaev, Gas-sensitive properties of thin film heterostructures based on $Fe_2O_3$–$In_2O_3$ nanocomposites, Sens. Actuators B: Chem. 93 (2003) 422–430.
[2] T. Takada, K. Suzuki, M. Nakane, Highly sensitive ozone sensor, Sens. Actuators B: Chem. 13 (1993) 404–407.
[3] T. Takada, H. Tanjou, T. Saito, K. Harada, Aqueous ozone detector using $In_2O_3$ thin-film semiconductor gas sensor, Sens. Actuators B: Chem. 25 (1995) 548–551.
[4] E.E. Gutman, Ozone sensor for the earth ozonosphere investigations, Sens. Actuators B: Chem. 25 (1996) 135–146.
[5] M. Ristic, S. Popovich, M. Tonkovich, Chemical and structural properties of the system $Fe_2O_3$–$In_2O_3$, J. Mater. Sci. 26 (1991) 4225–4233.
[6] E.E. Gutman, T.V. Belysheva, F.Kh. Chibirova, Structure effects in gas sensing by metal oxides, in: Proc. XI Europ. Conf. on Solid-State Transducers (EUROSENSORS XI), vol. 1, Poland, Warsaw, 21–24 September, 1997, pp. 341–344.
[7] F.Kh. Chibirova, E.E. Gutman, Structural defects and gas-sensing properties of some semiconducting metal oxides, Russ. J. Phys. Chem. 74 (9) (2000) 1555–1561.
[8] V.I. Goldanski, Chemical Application of Mössbauer Spectroscopy, Mir, Moscow, 1980, pp. 167–177.
[9] Y.S. Kang, S. Risbud, J.F. Rabolt, Synthesis and characterization of nanometer-size $Fe_3O_4$ and γ-$Fe_2O_3$ particles, Chem. Mater. 8 (1996) 2209–2211.
[10] G.N. Kryukova, A.N. Shmakov, S.V. Tsybulya, A.L. Chuvilin, L.P. Solovyeva, V.A. Sadykov, Vacancy ordering in γ-$Fe_2O_3$: synchrotron X-ray powder diffraction and high-resolution electron microscopy studies, J. Solid State Chem. 89 (1990) 208–211.
[11] F. Xu, X. Zhang, Y. Xie, Morphology control of γ-$Fe_2O_3$ nanocrystals via PEG polymer and accounts of its Mössbauer study, J. Colloid Interface Sci. 260 (1) (2003) 160–165.
[12] R.M. Cornell, R. Giovanoli, W. Shneider, Review of the hydrolysis of iron(III) and the crystallization of amorphous iron(III) hydroxide hydrate, J. Chem. Technol. 46 (1989) 115–134.
[13] A. Mandelis, C. Christofides, Physics, Chemistry and Technology of Solid State Gas Sensor Devices, John Wiley & Sons, New York, 1993, pp. 118–146.
[14] T. Belin, N. Guigue-Millot, J.P. Bellat, J.C. Niepce, Influence of grain size, oxygen stoichiometry, and synthesis conditions on the γ-$Fe_2O_3$ vacancies $Fe_2O_3$ and lattice parameters, J. Solid State Chem. 163 (2002) 459–465.
[15] G. Ennas, G. Marongui, A. Musinu, A. Falqui, P. Ballirano, R. Caminiti, Characterization of nanocrystalline γ-$Fe_2O_3$ prepared by wet chemical method, J. Mater. Res. 14 (4) (1999) 1570–1575.
[16] M. Ivanovskaya, D. Kotsikau, G. Faglia, P. Nelli, Influence of chemical composition and structural factors of $Fe_2O_3$/$In_2O_3$ sensors on their selectivity and sensitivity to ethanol, Sens. Actuators B: Chem. 96 (2003) 498–503.
[17] N. Yamazoe, New approaches for improving semiconductor gas sensors, Sens. Actuators B: Chem. 5 (1991) 7–19.
[18] O.V. Krylov, The Catalysis by Non-metals. The Appropriateness of the Catalysts Selection, Khimia, Leningrad, 1967, pp. 98–117.

[19] G.I. Golodets, Reductive–oxidative and acid–base steps of heterogeneous catalytic oxidizing reaction, catalysis mechanism, part 1, Nauka, Novosibirsk, 1984, pp. 142–158.
[20] A. Gurlo, N. Barsan, M. Ivanovskaya, U. Weimar, W. Göpel, $In_2O_3$ and $In_2O_3$–$MoO_3$ thin film semiconductor sensors: interaction with $NO_2$ and $O_3$, Sens. Actuators B: Chem. 47 (1998) 92–99.
[21] M. Ivanovskaya, P. Bogdanov, G. Faglia, G. Sbervrglieri, The features of thin film and ceramic sensors for the detection of CO and $NO_2$, Sens. Actuators B: Chem. 68 (2000) 344–350.
[22] M. Ivanovskaya, P. Bogdanov, G. Faglia, P. Nelli, G. Sbervrglieri, On the role of catalytic additives in gas-sensitivity of $SnO_2$-based thin film sensors, Sens. Actuators B: Chem. 70 (2001) 268–274.

## Biographies

**Dr. Maria I. Ivanovskaya** received her degree in chemistry in 1980 from the Belarusian State University in the field of photochemistry. Since 1989 she has been working at the Research Institute for Physical Chemical Problems of the Belarusian State University. Her main scientific interest is solid state chemistry in applications to catalysis and semiconductor gas sensors, structural features of nanosized oxides ($SnO_2$, $MoO_3$, $In_2O_3$, $Fe_2O_3$, $CeO_2$, $ZrO_2$, $La_2O_3$) and oxide composites.

**Dr. Dzmitry A. Kotsikau** received his degree in chemistry in 2005 from Belarusian State University in the field of semiconductor gas sensors. Now he is working at the Research Institute for Physical Chemical Problems of the Belarusian State University in the field of semiconductor gas sensors and catalysts. His main scientific interests are $Fe_2O_3$–$In_2O_3$ and $Fe_2O_3$–$SnO_2$ nanosized composites, their structural and gas-sensitive characterization.

**Dr. Antonietta Taurino** took her PhD in physics in 1999 at the University of Lecce. Since 2001 she has been working as researcher at the Institute for Microelectronics and Microsystems of CNR. Her competences are related to the analysis of the morphological, structural and compositional properties of materials by transmission electron microscopy techniques, scanning transmission electron microscopy (STEM), electron beam induced current (EBIC), as well as by new techniques for nano-manipulation of materials by FIB. The main fields of interest are nanostructured thin films of single and mixed metal-oxides for gas sensors and III–V low dimensional semiconductors for optoelectronics.

**Dr. Pietro Siciliano** received his degree in physics in 1985 from the University of Lecce. He took his PhD in physics in 1989 at the University of Bari. During the first years of activities he was involved in research in the field of electrical characterization of semiconductors devices. He is currently working in the field of preparation and characterization of thin film for gas sensor and multisensing systems.